Atomic Spectroscopy

Article

Determination of Radioactive Selenium-79 in Environmental Samples by ICP-MS after Solid Phase Microextraction - Dielectric Barrier Discharge Vapor Generation

Zhenqi Gao, [a] Shanshan Chen, [a] Zenghui Zhu, [a] Junrong Wang, [a] Shengkang Liang, [b] and Qian He [b,*]

[a] College of Chemistry and Chemical Engineering, Ocean University of China, Qingdao, 266100, P. R. China

[b] Frontiers Science Center for Deep Ocean Multispheres and Earth System, and Key Laboratory of Marine Chemistry Theory and Technology, Ministry of Education, Ocean University of China, Qingdao 266100, P. R. China

Received: *June 02, 2026;* ***Revised:*** *August 10, 2026;* ***Accepted:*** *August 16, 2026;* ***Available online:*** *August 16, 2026.*

DOI: 10.46770/AS.2026.0038

ABSTRACT: Accurate determination of ^{79}Se level in environmental samples is critical for evaluating radioactive contamination risk. A new pretreatment method for ^{79}Se determination by inductively coupled plasma-mass spectrometry (ICP-MS) through solid phase microextraction (SPME) - dielectric barrier discharge vapor generation (DBDVG) - ammonia water absorption-evaporation (AAE) was proposed in this work. The sorbent of nano-ZrO_2 was used in SPME, which could both enrich Se and selectively adsorb Se from Br, which has an identical mass of 79 to ^{79}Se. DBDVG was used to reduce the species of Se from Se(IV) or Se(VI) to volatile H_2Se vapor to eliminate the sample matrix interferences. Ammonia water was used to absorb the volatile H_2Se and then evaporated to enrich Se. The adsorption, DBDVG and absorption parameters were optimized in detail. The mass interference of $^{38}Ar^{40}ArH^+$ was effectively eliminated by the addition of He gas in the collision/reaction cell, and the other potential interferences of $^{39}K^{40}Ar^+$, $^{63}Cu^{16}O^+$, $^{158}Gd^{2+}$, $^{158}Dy^{2+}$ and $^{78}SeH^+$ were all not obvious in this method. The detection limit of ^{79}Se was 10.1 ng L^{-1} and the inter-batch reproducibility between different SPME tubes was 1.9 %. The concentration of ^{79}Se in environmental samples such as lake water and plant leaves were assessed. Compared with conventional ion exchange resin methods for enrichment of ^{79}Se, our SPME approach achieves desorption via DBD plasma without the need of acidic or alkaline reagent for elution. In contrast to conventional ICP-MS sample introduction methods for ^{79}Se determination, such as hydride generation and electrothermal vaporization, the proposed DBDVG technique drives redox reactions entirely via free radicals and electrons generated in the discharge plasma. This design fully eliminates the need for additional redox reagents or chemical modifiers, and thus drastically lowers the associated reagent blank levels.

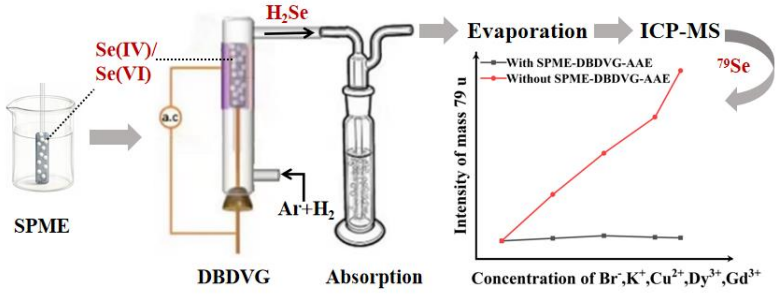

INTRODUCTION

Selenium-79 (^{79}Se) is a pure β^- emitter that decays directly to the ground state of ^{79}Br. It is primarily generated in nuclear reactors via the spontaneous fission of uranium-235, with a relatively low fission yield of 0.04%.[1] Owing to its long half-life (2.8×10^5 - 3.77×10^5 years),[1-3] high environmental mobility,[4] and inherent toxicity, ^{79}Se is recognized as a key radioactive pollutant, which is of great relevance to the decommissioning of nuclear facilities, the safe management of nuclear waste, and the comprehensive assessment of environmental radioactivity.[5,6] Accurate determination of ^{79}Se level in environmental samples is therefore critical for evaluating radioactive contamination risks, safeguarding ecological security, and supporting the formulation of sound nuclear environmental management strategies.

The conventional techniques for ^{79}Se determination include liquid scintillation counting (LSC),[7-11] accelerator mass spectrometry (AMS)[12-14] and inductively coupled plasma mass spectrometry (ICP-MS).[15-18] Among these, the pretreatment steps for LSC determination of ^{79}Se are always complex and time-consuming, which contains resin separation, extraction, reduction, precipitation, re-dissolution, or distillation, etc, [7-11] as ^{79}Se could only be measured after removing interfering activity from ^{137}Cs, ^{90}Sr, ^{99}Tc, ^{147}Pm, ^{151}Sm, ^{93}Zr, etc, whose β-decay spectra could appear similar to that of ^{79}Se, and whose content would be expected at levels near or greater than ^{79}Se. Meantime, the analysis time of ^{79}Se by LSC is also long due to the long half-time of ^{79}Se. For AMS determination, although the detection limit of ^{79}Se could be better than 1.0×10^{-12},[14] the price of AMS is very high, which could not be used for routine analysis. Thus, ICP-MS is a suitable alternative for measuring such long-lived radionuclide, attributed to its high sensitivity, short analysis time, and relatively simple pretreatment process.[1, 15-18]

However, several atomic and molecular ions arising from the sample matrix ($^{79}Br^+$, $^{39}K^{40}Ar^+$, $^{63}Cu^{16}O^+$, $^{158}Gd^{2+}$, $^{158}Dy^{2+}$) itself and the plasma gas ($^{38}Ar^{40}ArH^+$) can interfere with the $^{79}Se^+$ ions determined by ICP-MS. To solve the interferences from sample matrix, the pretreatment technique of solid–phase extraction with ion exchange resin,[1,15,16,18] and the sample introduction techniques of hydride generation (HG)[2,17] and electrothermal vaporization (ETV)[1,15] had been proposed to remove the potential isobaric interferences for ^{79}Se determination. Ion exchange resin relies on fixed charged functional groups on their skeletons to undergo equicharge reversible substitution with oppositely charged ions in solution, thereby achieving adsorption of target ions such as Se(IV)[19] and separation of impurities. HG refers to the process in which borohydride reacts with Se(IV) under acidic conditions to convert it into volatile H_2Se vapor, which enables the effective separation of Se from the sample matrix.[20,21] And ETV refers to a thermal separation program to reduce the matrix before the introduction of Se into the plasma. Nevertheless, the interferences of $^{79}Br^+$ could not be removed either by ion exchange resin (such as AG50w-X8) or HG and ETV sample introduction systems.[2,15,17] To eliminate the interference of $^{79}Br^+$, Aguerre and Frechou[16] found that evaporation, precipitation of silver halides and elution on anion exchange resin with certain condition could be used for separation Se from Br. Banjarnahor et al[22] found that activated alumina could remove Br from Se in the presence of nitrate and carbonate, which strongly competed with Br^- and allowed the Br^- to pass through the sorbent. Besides, the collision/reaction cell (CRC) with an appropriate reaction gas such as NH_3,[22] N_2O/NH_3[23] and O_2/He[24] by ICP-MS or ICP-MS/MS have been proposed for separation of $^{79}Br^+$ and $^{79}Se^+$ as well as $^{38}Ar^{40}ArH^+$, with the separation factor higher than seven orders of magnitude between $^{79}Br^+$ and $^{79}Se^+$.[23]

Herein, we proposed a new pretreatment method for ^{79}Se determination by four steps: solid phase microextraction (SPME)[25] - dielectric barrier discharge vapor generation (DBDVG)[26,27] - ammonia water absorption-evaporation (AAE) before determination by ICP-MS. In this method, nano-ZrO_2 was used as sorbent in SPME, which can both enrich Se[28,29] and selectively adsorb Se from Br in solution. DBDVG was used to reduce the species of Se from Se(IV) or Se(VI) to volatile H_2Se to eliminate the sample matrix interferences.[26,27] Ammonia water was used to absorb the volatile H_2Se and then evaporated to enrich Se. Compared with the conventional ion exchange resin methods,[15,16,18] our method of SPME is performed with desorption driven by DBD plasma discharge without elution by acidic or alkaline reagents[27,30] and the adsorbent of nano-ZrO_2 not only can adsorb Se, but also can separate Br. Compared with HG[2,17] and ETV[1,15] sample introduction methods, our method of DBDVG realizes redox reactions through free radicals and electrons in the plasma,[31] with no need to add extra redox reagents in HG or chemical modifiers in ETV, which greatly lowers the reagent blank. In this work, the separation condition of Br and Se as well as the adsorption condition of Se by nano-ZrO_2 were investigated in detail. Meantime, the matrix interferences of $^{39}K^{40}Ar^+$, $^{63}Cu^{16}O^+$, $^{158}Gd^{2+}$, $^{158}Dy^{2+}$ and the plasma gas interferences of $^{38}Ar^{40}ArH^+$ were also evaluated. Based on these studies, the suitability of using ICP-MS as a sensitive method for the determination of ^{79}Se in environmental sample was assessed.

EXPERIMENTAL

Reagents and materials. The reagents used in this experiment were at least analytical reagent grade. Ultrapure deionized water (18.2 MΩ cm, obtained from Millipore milli-Q ELIX Advantage System, USA) was used throughout the experiment. High-purity argon (Ar) gas (99.999%) and helium (He) gas (99.999%) were all supplied by Qingdao Zesheng Energy Co., Ltd., China. High-purity hydrogen (H_2) gas (99.999%) was generated from a hydrogen generator (Beijing Zhongkejirui Technology Co., Ltd, China). The Ar-H_2 mixture was configured by controlling the flow rates of the two high-purity gases through two rotameters (0~600 mL min^{-1}; 25~250 mL min^{-1}, Yuyao Yinhuan Flowmeter Co., Ltd, China). Nano-ZrO_2 (purity: 99.99 wt%, particle size: <100 nm) was purchased from Shanghai Aladdin Biochemical Technology Co., Ltd (China). The solid chemicals of $Cu(NO_3)_2$, KCl, NaBr and NaOH were purchased Sinopharm Chemical Reagent Co., Ltd. (China) as well as absolute ethanol. Phenol-formaldehyde (PF) resin was purchased from Shanghai Maclin Biochemical Technology Co., LTD (China). Nitric acid and ammonia water with trace elemental level were all purchased from Merck Drugs & Biotechnology (Germany). Hydrogen peroxide (30%, v/v) was purchased from Sinopharm Chemical Reagent Co., Ltd. (China). The standard solutions of Gd (GSB 04-1780-2004) and Dy (GSB 04-1782-2004) were purchased from National Center of Analysis and Testing for Nonferrous Metals and Electronic Materials

(China). The standard solutions of Se(IV) (BWB2505-2016) and Se(VI) (BWB2577-2016) were purchased from the Beijing North Weiye Institute of Metrology Technology, China. A series of working solutions for Se(IV) and Se(VI) were prepared by diluting the standard solution with nitric acid solution. The Se isotopic reference material in selenious acid solutions (GBW 04457, GBW 04456, GBW 04449, National Institute of Metrology, China) were used to evaluate the mass fractionation effect and the accuracy of the method. To validate the applicability of the methodology, plant leaves of rohdea japonica and lake water collected from our university campus were assessed.

Instrumentation. The DBDVG configuration was implemented as detailed in our previous work.[27] In brief, the DBD reactor comprised two concentric glass components: (1) an inner glass tube (sealed at one end; 2 mm i.d × 3 mm o.d × 70 mm length) containing an internal copper wire electrode, and (2) an outer glass tube (8 mm i.d× 10 mm o.d × 100 mm length) wrapped with a 40 mm copper foil electrode. Electrodes were powered by an ozone-generator compatible supply (Anhui Tianze Electronic Technology Co., LTD, China) with a frequency of 45 kHz and the input discharge voltage of 250 V. An ICP-MS (iCAP Q, Thermo Fisher Scientific, Germany) was used for Se determination throughout the experiments. Kinetic energy discrimination (KED) mode in CRC with He gas was used to reduce the polyatomic interferences for ^{79}Se determination. The optimized conditions for ICP-MS experimental parameters were listed in Table S1. A scanning electron microscopy energy dispersive X-ray fluorescence spectrometer (SEM-EDS, Gemini SEM 360, ZEISS, Germany) were used to characterize the elemental composition of nano-ZrO_2 before and after adsorption. An atomic fluorescence spectroscopy (AFS, PF3 Beijing Persee Instrument Co., Ltd., China) was used to characterize the memory effect of Se by DBD desorption and vapor generation.

Analytical procedure. The preparation process of the nano ZrO_2-coated SPME tube was shown in Fig. 1a. 3 g of nano-ZrO_2 and 0.2 g of PF resin were added into 10 mL of absolute ethanol, followed by 2 h of room-temperature sonication to yield a uniform dispersion. A clean SPME glass tube was then vertically inserted in the mixture and withdrawn slowly, resulting in the formation of a nano-ZrO_2 coating on its outer surface. Finally, the coated tube was placed on a hot plate and cured at 150 °C for 3 h to remove residual solvent. The SPME, DBDVG, ammonia water absorption and evaporation processes for ^{79}Se determination were shown in Fig. 1b. A nano-ZrO_2 coated SPME tube was inserted into 50 mL of Se standard solution or sample solution to adsorb Se for 2 h. Then, the SPME tube was taken out and placed in the air for 30 min to reduce moisture. Subsequently, the SPME tube was inserted into the DBD reactor as the inner glass tube and hermetically sealed. Upon introducing a mixed Ar/H_2 gas flow and activating the power supply, DBD plasma was instantly generated—this step enabled simultaneous Se desorption and vapor generation. The resulting H_2Se vapor was bubbled into 30 mL of 1% (v/v) ammonia water for absorption, then concentrated to near dryness on a hot plate at 80 °C for approximately 10 h. Finally, the dried residue was redissolved in 2 mL of nitric acid (pH=1), and the Se contents such as ^{77}Se and ^{79}Se were analyzed by nebulization ICP-MS.

The desorption and vapor generation efficiency of Se by DBD was quantified through determining the content of Se in nano-ZrO_2 on the adsorption tube before and after the DBD processing. The Se content in nano-ZrO_2 before DBD processing was calculated from the adsorption efficiency and the original Se content. For the residual Se content in nano-ZrO_2 after DBD processing, the nano-ZrO_2 was transferred into 10 mL of eluent (0.5 M NaOH and 2% (v/v) H_2O_2), vigorously vibrating for 1.5 h to sufficient leach out the residual Se,[32] after which the Se concentration was determined by ICP-MS.

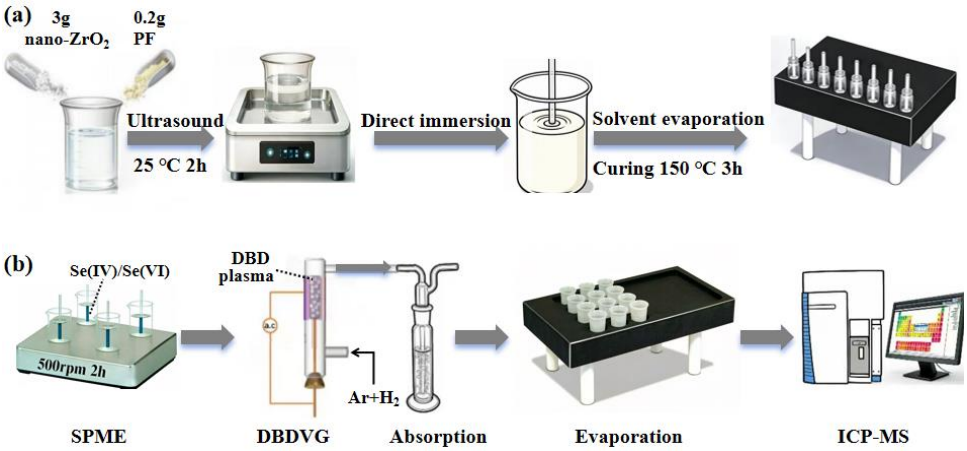

Fig. 1 Schematic diagram of the experimental setup. (a) The preparation process of nano-ZrO_2 coated SPME tube. (b) The SPME adsorption, DBD desorption/vapor generation, ammonia water absorption and evaporation processes for ^{79}Se determination by ICP-MS.

RESULTS AND DISCUSSION

Adsorption of Se by nano-ZrO_2 by SPME. To validate the adsorption behavior of nano-ZrO_2 toward Se, SEM-EDS was used to characterize the ZrO_2 coating before and after the adsorption of Se(IV). The EDS analysis results showed that before adsorption, the coating was mainly composed of Zr, O and a small amount of C, and no characteristic signal of Se was detected (Fig. 2a). After the adsorption treatment, obvious peak appeared in the characteristic energy range of Se in the spectrum (Fig. 2b), which proved that Se had been successfully adsorbed on the nano-ZrO_2 coated SPME tube.

Subsequently, the effect of adsorption conditions such as adsorbent concentration, rotate speed, and adsorption time on the adsorption efficiency of nano-ZrO_2 for Se(IV) (10 μg L^{-1}) were investigated. To reduce the inherent Se background of the nano-ZrO_2 adsorbent, this material was pretreated with at least three DBD plasma discharge cycles to eliminate Se interference prior to adsorption. The final Se blank was below 0.1% of the signal from 10 μg L^{-1} Se(IV). The adsorption efficiency (η_1) of Se(IV) was measured by ICP-MS using the eq. (1):

$$\eta_1 = (1 - m_a/m_b) \times 100\% \quad (1)$$

where m_b and m_a were the contents of Se in the solution before and after adsorption, respectively. As shown in Fig. 3a, the adsorption efficiency rose rapidly as the nano-ZrO_2 concentration increased from 0 to 0.1 g mL^{-1}. Then the adsorption rate climbed slightly as the concentration rose to 0.3 g mL^{-1} and reached the plateau after the concentration surpassed 0.3 g mL^{-1}. As shown in Fig. 3b, the adsorption efficiency increased with the increase of the rotation speed and reached a plateau at the rotation speed higher than 500 rpm. Meantime, as shown in Fig. 3c, the adsorption efficiency gradually increased within the adsorption time of 120 min (2 h) and reached a plateau after 2 h, indicating that the adsorption basically reached equilibrium with the adsorption time higher than 2 h.

Furthermore, as the surface charge of nano-ZrO_2 is different at different pH values,[29] which may show different adsorption capacities for Se(IV) as well as Se(VI), the effect of solution pH of nano-ZrO_2 for the adsorption efficiency of Se(IV) and Se(VI) was also studied. Among this experiment, 2 % (v/v) nitric acid and 2 % (v/v) ammonia water were used to adjust the solution pHs. As shown in Fig.3d, the adsorption efficiencies for two species were both high under acidic conditions, with the highest efficiency at pH =1, and significantly low under alkaline conditions. Under acidic conditions, Se(IV) is immobilized on ZrO_2 via coordination bonding, whereas Se(VI) is captured through electrostatic interactions; both species exhibit high and nearly consistent adsorption efficiencies. Under alkaline conditions, OH^- competes with Se(IV) for available surface sites on ZrO_2, and the electrostatic attraction between Se(VI) and the adsorbent vanishes,

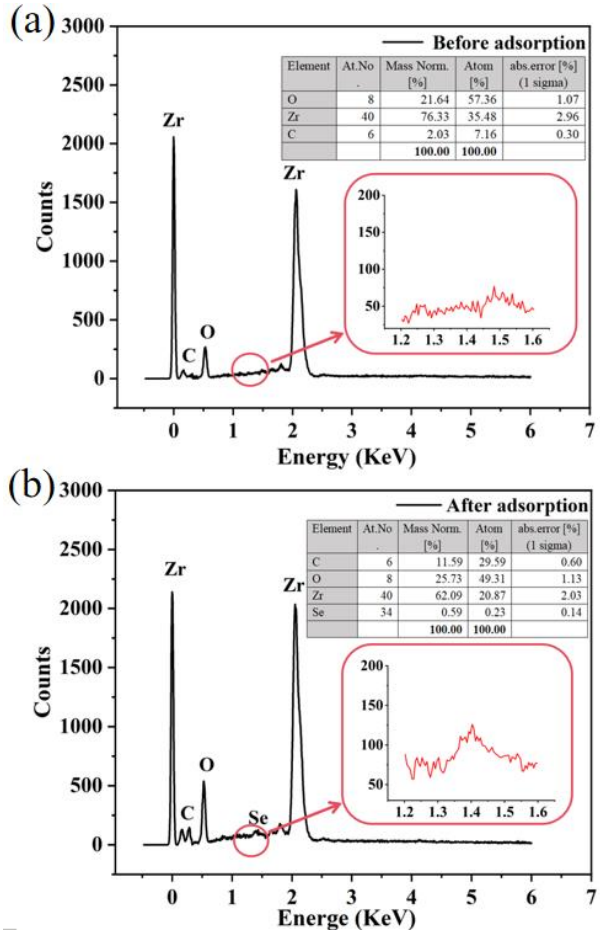

Fig. 2 The SEM-EDS spectra of nano-ZrO_2 (0.3 g mL^{-1}) before (a) and after (b) adsorption of Se(IV) (1000 mg L^{-1}).

leading to a drastic drop in adsorption efficiency for both selenium species.

From the above results, to achieve the highest adsorption efficiency, the adsorbent concentration of 0.3 g mL^{-1}, rotate speed of 500 rpm, adsorption time of 2 h and acid condition (pH=1) were adopted for total Se adsorption. Among these parameters, adsorbent dosage and rotate speed are mass transfer-related variables, which can only accelerate the adsorption process by increasing the diffusion rate of Se(IV) toward the adsorbent particle surface, rather than altering the intrinsic thermodynamic adsorption equilibrium limit. In contrast, sufficient adsorption time provides a necessary precondition for the system to reach this equilibrium state, while solution pH modulates the interfacial reaction conditions, making these two parameters the core factors that determine whether the system can achieve its theoretical maximum adsorption efficiency. Under the optimized conditions, the highest adsorption efficiencies of Se(IV) and Se(VI) were calculated as 95.4±2.7 %. For convenience, Se(IV) will be used for subsequent research unless otherwise specified.

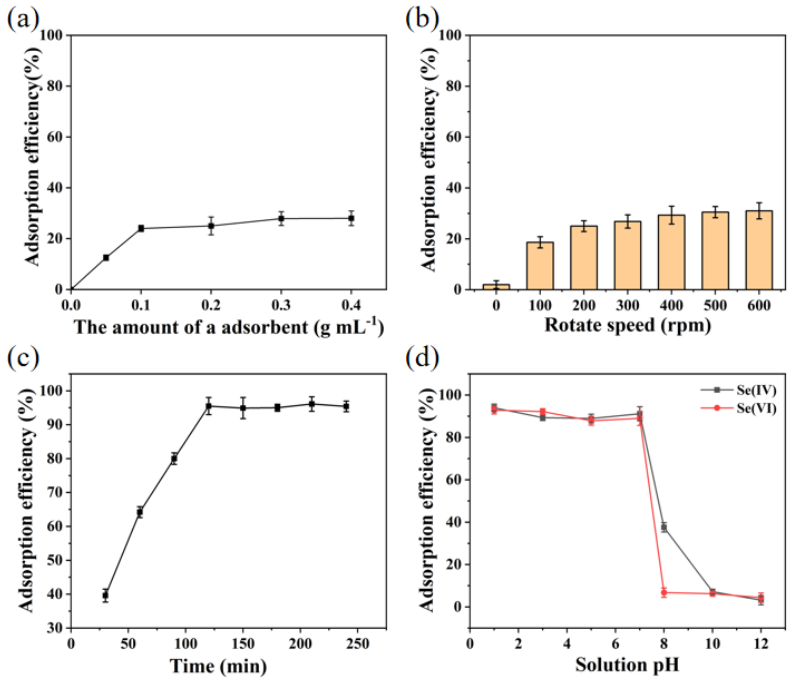

Fig. 3 Effect of adsorbent concentration (a), rotate speed (b), adsorption time (c) on the adsorption efficiency of Se(IV) (10 μg L^{-1}), and solution pH (d) on the adsorption efficiency of Se(IV) and Se(VI) (10 μg L^{-1}) by nano-ZrO_2. Each data is the average of three measurements (n=3). Error bars are defined as ± SD.

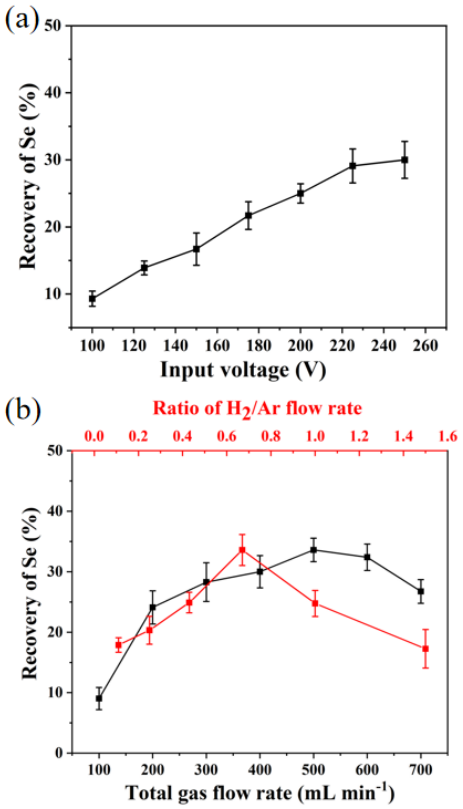

Fig. 4 Effect of input discharge voltage (a) and total gas flow rate and ratio of H_2/Ar carrier gas (b) of DBDVG on recovery of Se with original Se(IV) concentration of 10 μg L^{-1}. Each data is the average of three measurements (n=3). Error bars are defined as ± SD.

Desorption and vapor generation of Se(IV) by DBDVG. Since the plasma may deposit Se or other metals on surfaces, the memory effect of Se(IV) desorption and vapor generation by DBDVG was first studied by directly determination of H_2Se vapor through AFS. As shown in Fig. S1, the Se peak intensity in the second discharge decreased significantly compared with the first discharge, indicating that effective desorption and vapor generation of Se(IV) on nano-ZrO_2 could be achieved by first discharge and the memory effect was not obvious. To optimize the desorption and vapor generation efficiency of Se(IV) in the DBDVG step, the effects of input discharge voltage and carrier gas flow rate were systematically investigated, and the evaluation was carried out by calculating the recovery of Se in ammonia water solution with the same absorption conditions. The recovery of Se (η_2) was measured by ICP-MS using the eq. (2):

$$\eta_2 = (m_c/m_d) \times 100\% \quad (2)$$

where m_c and m_d were the contents of Se in ammonia water after DBDVG-AAE processing and in nano-ZrO_2 before DBDVG-AAE processing, respectively.

The input discharge voltage directly affects the DBD plasma intensity.[30] As shown in Fig. 4a, within the range of 100-250 V, the recovery of Se increased obviously with the increase of the discharge voltage. This result indicates that increasing the voltage is beneficial for enhancing the desorption of Se(IV) and its reduction to H_2Se by the DBD plasma. Considering the range limit

of the voltage transformer and the safety of the experiment, the voltage higher than 250 V was not studied, and 250 V was selected for the following experiment.

Ar gas provides the DBD plasma discharge environment and H_2 gas is beneficial to the reduction of Se(IV) to H_2Se.[27,33,34] As shown in Fig. 4b, under the condition of a fixed H_2/Ar ratio (2:3), the highest recovery of Se appeared at the total gas flow rate of 500 mL min^{-1}. Meantime, when the total gas flow rate was fixed at 500 mL min^{-1}, the highest recovery of Se appeared with the H_2/Ar gas flow ratio of 0.67. Finally, Ar gas flow rate of 300 mL min^{-1} and H_2 gas flow rate of 200 mL min^{-1} were chosen for subsequent study.

Absorption of H_2Se vapor by ammonia water. In order to reduce the generation efficiency of molecular ions interference caused by H_2 for ^{79}Se determination such as $^{38}Ar^{40}ArH^+$ and $^{78}SeH^+$, we did not introduce the gaseous products including H_2Se, H_2, etc after DBD desorption and vapor generation into ICP-MS directly. Instead, we used ammonia water for absorption, then evaporated it to dryness and redissolved it by HNO_3 (pH=1) before determination by ICP-MS. To optimize the absorption efficiency of H_2Se vapor by ammonia water, the effects of ammonia water volume, absorption time, and ammonia water concentration on the recovery of Se (η_2) were also investigated.

As shown in Fig. 5a, as the volume of ammonia water increased, the recovery of Se rose gradually and decreased slightly once the volume went beyond 30 mL. This trend may be attributed to the limited available absorption interface or local saturation at small solution volumes, which results in lower absorption efficiency. In contrast, absorption time (5-20 min) had little effect on the recovery of Se (Fig. 5b). This phenomenon could be attributed to the near-instantaneous completion of the desorption and vapor generation process via DBDVG, which permits nearly all H_2Se vapor to be released within a short time. Meanwhile, the concentration of ammonia water also affected the recovery of Se (Fig. 5c). The recovery of Se rose steadily from 0 to 1 % (v/v) of ammonia water, then followed by a marginal drop at 10 % (v/v), which confirmed 1 % (v/v) of ammonia water was adequate to react with H_2Se. Therefore, 30 mL of ammonia water (1%, v/v) with the absorption time of 5 min were adopt for the following study. The highest recovery of Se was calculated as 48.9±2.2 %, which may be limited by the desorption and vapor generation efficiency (52.2±1.5 %) of Se(IV) by DBDVG from the SPME tube.

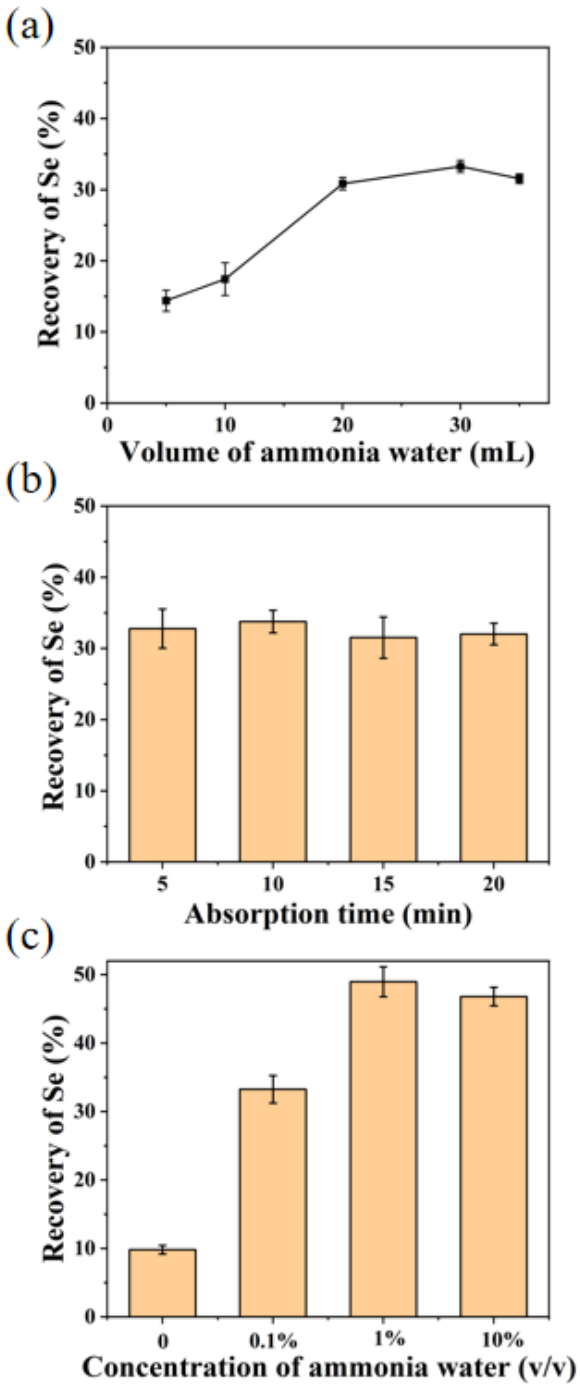

Fig. 5 Effect of volume (a), absorption time (b) and concentration (c) of ammonia water on recovery of Se with original Se(IV) concentration of 10 μg L^{-1}. Each data is the average of three measurements (n=3). Error bars are defined as ± SD.

The mass interference of ^{79}Br for ^{79}Se. Since ^{79}Br has the same mass number as ^{79}Se, it will cause serious isobaric interference to ^{79}Se. We first investigated the adsorption efficiency of Br^- by nano-ZrO_2 and compared it with Se(IV). As shown in Fig. 6a, under the same conditions, the adsorption efficiency of Se(IV) reached 95%, but the adsorption efficiency of Br^- was below 3%, indicating that nano-ZrO_2 could selectively adsorb Se from Br. The adsorption difference may be due to the fact that compared with Br^-, Se(IV) has higher charge, lower hydration energy, and stronger coordination ability with ZrO_2.

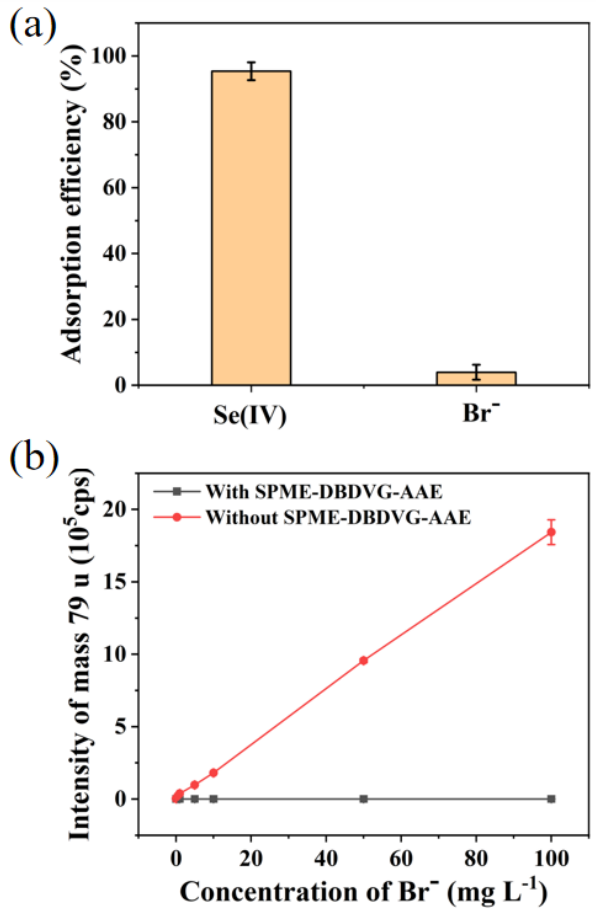

Fig. 6 (a) Comparison of adsorption efficiency between Se(IV) and Br^- using nano-ZrO_2 by SPME with the same concentration of Se(IV) and Br^- of 10 μg L^{-1}. (b) The signal intensities at the mass number of 79 u in ICP-MS with and without the pretreatment process of SPME-DBDVG-AAE under the same Br^- concentration. Each data is the average of three measurements (n=3). Error bars are defined as ± SD.

Then the signal intensities at the mass number of 79 u in ICP-MS with and without the pretreatment process of SPME-DBDVG-AAE under the same initial Br^- concentration were also compared. As shown in Fig. 6b, with the increase of Br^- concentration, the signal values of 79 u were increased linearly without the pretreatment process, while the signal values of 79 u were close to the blank signal value with the pretreatment process and the signal values of 79 u were not affected by the Br^- concentrations in the solution. These results indicated that our proposed SPME-DBDVG-AAE method can effectively eliminate the interference of ^{79}Br for ^{79}Se determination in the sample.

The mass interferences of other atomic and molecular ions for ^{79}Se. Except ^{79}Br, the other interfering ions on mass number of 79 u such as $^{38}Ar^{40}ArH^+$, $^{39}K^{40}Ar^+$, $^{63}Cu^{16}O^+$, $^{158}Gd^{2+}$, $^{158}Dy^{2+}$ and $^{78}SeH^+$ were also tested. To eliminate the interference of $^{38}Ar^{40}ArH^+$, the KED mode in CRC with He gas and a lower RF power of 1000 W in ICP-MS were used. The effect of He gas flow rate on the signal intensity of mass number of 79 u caused by $^{38}Ar^{40}ArH^+$ with HNO_3 (pH=1) solution blank was tested. As shown in Fig. 7a, when the flow rate of He gas was less than 1.5 mL min^{-1}, there was not only no collision effect, but also the slight collision focusing might improve the transmission of target ions, resulting in an abnormal increase in the signal value. Only when the flow rate of He gas exceeded 2.5 mL min^{-1} could an obvious collision effect be observed. When the flow rate of He gas was higher than 4.5 mL min^{-1}, the signal value of $^{38}Ar^{40}ArH^+$ was close to zero. In order to take into account of the sensitivity of ^{79}Se simultaneously, we also investigated the effect of He gas flow rate on the signal of ^{77}Se instead of ^{79}Se with 10 μg L^{-1} of Se(IV) solution. As shown in Fig. 7a, when the He flow rate reached 3.5 mL min^{-1}, both the sensitivity of ^{77}Se (~645 cps/(μg L^{-1})) and the blank signal of 79 u (~200 cps) fall within acceptable ranges. Therefore, a He gas flow rate of 3.5 mL min^{-1} was chosen to simultaneously balance the interference removal of $^{38}Ar^{40}ArH^+$ and the sensitivity of ^{79}Se.

Then the interferences of $^{39}K^{40}Ar^+$, $^{63}Cu^{16}O^+$, $^{158}Gd^{2+}$, $^{158}Dy^{2+}$ from the sample matrix for ^{79}Se determination were further studied. As shown in Fig.7b-e, with the increase in the concentrations of K^+, Cu^{2+}, Gd^{3+} and Dy^{3+}, if there was no pre–treatment process of SPME-DBDVG-AAE, obvious signal values were observed at the mass number of 79 u, and the signal values were greatly affected by the concentrations of these interfering ions. However, after the pre-treatment process of SPME-DBDVG-AAE, the signal values at the mass number of 79 u were comparable to those of the blank solution and were not affected by these interfering ions concentrations, indicating that the SPME-DBDVG-AAE process can effectively remove the interference of $^{39}K^{40}Ar^+$, $^{63}Cu^{16}O^+$, $^{158}Gd^{2+}$ and $^{158}Dy^{2+}$ for ^{79}Se determination.

In addition, it is worth noting that when the Se concentration is too high, the formation of $^{78}SeH^+$ may also interfere with the determination of ^{79}Se. Thus, we also investigated the influence of Se concentration on the signal intensity of ^{79}Se. As shown in Fig.7f, when the Se(IV) concentration was as high as 1 mg L^{-1}, the signal of mass number of 79 u was still close to the blank solution with the pretreatment process of SPME-DBDVG-AAE. These results indicated that within the concentration range of Se, the formation efficiency of $^{78}SeH^+$ was extremely low, and its interference for ^{79}Se could be neglected.

Analytical performance. Prior to linear calibration, the mass fractionation effect of Se isotopes with the pretreatment process of SPME-DBDVG-AAE was first investigated. As shown in Fig. S2, the isotope ratio drifts of $^{82}Se/^{76}Se$, $^{77}Se/^{82}Se$, $^{78}Se/^{76}Se$ and $^{78}Se/^{82}Se$, measured from three Se isotopic reference materials (GBW04457, GBW04456 and GBW04449) with and without the SPME-DBDVG-AAE pretreatment, were all insignificant. These results confirmed that the mass fractionation effect of Se isotopes

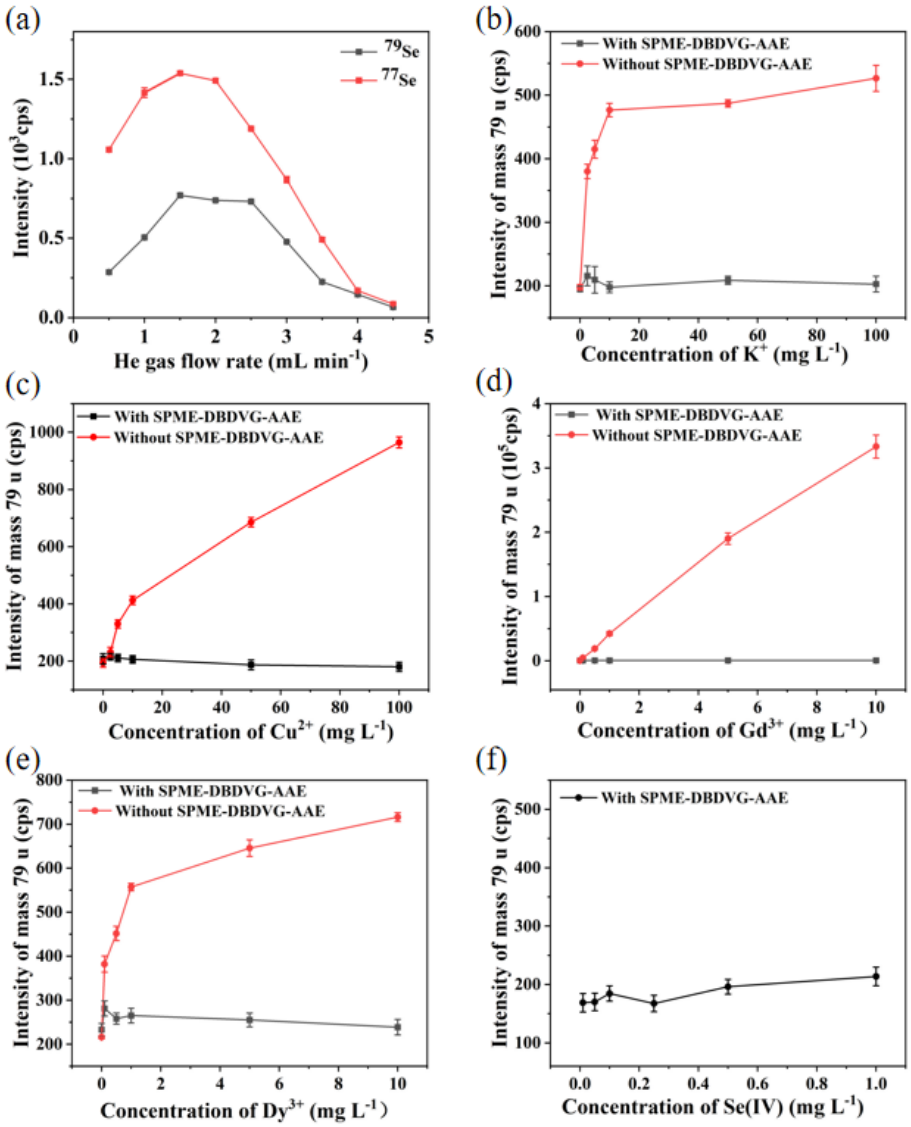

Fig. 7 (a) Effect of He gas flow rate in CRC on the interference of ^{79}Se by $^{38}Ar^{40}ArH^+$ with HNO_3 (pH=1) blank and the signal of ^{77}Se with 10 μg L^{-1} of Se(IV) solution; The comparison of the interference of $^{39}K^{40}Ar^+$ (b), $^{63}Cu^{16}O^+$(c), $^{158}Gd^{2+}$ (d) and $^{158}Dy^{2+}$ (e) on ^{79}Se determination with and without the pretreatment process of SPME-DBDVG-AAE; (f) The interference of $^{78}SeH^+$ on ^{79}Se determination under different concentrations of Se(IV) with the pretreatment process. Each data is the average of three measurements (n=3). Error bars are defined as ± SD.

introduced by the SPME-DBDVG-AAE pretreatment was negligible. Therefore, we used a non-radioactive Se standard with similar chemical behavior as ^{79}Se for the linear study, as no ^{79}Se standard is available for our work. The Se calibration curve was linear from 0 to 25 μg L^{-1}. Considering the natural abundance of the isotopes, the calibration was found to be linear from 0 to 2.33 μg L^{-1} for ^{76}Se, from 0 to 1.91 μg L^{-1} for ^{77}Se and from 0 to 5.94 μg L^{-1} for ^{78}Se. The average sensitivity was around 614 cps per μg L^{-1} for three Se isotopes (as shown in Fig. S3). Thus, the detection limit (LOD) of ^{79}Se was calculated as 10.1 ng L^{-1} using the definition 3 σ/m (σ is the standard deviation of 11 blank of the mass 79 u and m is the slope of the calibration curve, i.e. the average sensitivity mentioned above). The inter-batch reproducibility between different SPME adsorption tubes (n = 7) for Se determination was calculated as 1.9 % (Fig. S4a) and the reuse number of each SPME tube could be reused at least four times (Fig. S4b).

As shown in Table 1, compared with the conventional solid-phase extraction (SPE) with ion exchange resin methods,[15,22,10,35] our method of SPME is performed with desorption driven by DBD plasma without elution by acidic or alkaline reagents and the adsorbent of nano-ZrO_2 not only can adsorb Se but also can separate Br. Compared with HG,[17] ETV[15] and distillation[11]

Table 1. The comparison of different methods for ^{79}Se determination

Method	LOD of ^{79}Se (ng L^{-1})	Elution reagent	Vaporization reagent	Gas in CRC	Reference
HG-ICP-MS	100	—	$HCl/NaBH_4$	—	17
SPE-ETV-ICP-MS	13	HNO_3	$Pd(NO_3)_2$	—	15
SPE-ICP-MS/MS	1.2	HNO_3/NaOH	—	NH_3/He	22
ICP-MS/MS	0.17	—	—	NH_3/N_2O	23
Precipitation-SPE-precipitation-LSC	88.1[a]	HNO_3	—	—	10
Distillation-precipitation-LSC	0.9[b]	—	HCl/HBr	—	11
NEMI/EPA Method RP530	—	HNO_3/HBr	—	—	35
Precipitation-AMS	1.6	—	—	—	14
SPME-DBDVG-AEE-ICP-MS	10.1	Free	Free	He	This work

Note: [a] Converted from 0.05 Bq/g with ^{79}Se half-life of 2.95×10^5 years; [b] Converted from 0.52 Bq/L with ^{79}Se half-life of 2.95×10^5 years.

Table 2. Analytical results of ^{77}Se and ^{79}Se concentrations in environment samples by SPME-DBDCVG-AAE-ICP-MS method (n = 5)

Sample	Determined value		^{77}Se added value	^{77}Se recovery
	^{77}Se	^{79}Se		
Lake water	0.055 ± 0.007 μg L^{-1}	ND	0.5 μg L^{-1}	99.9±4.1 %
Plant leaves	0.0041 ± 0.0003 μg g^{-1}	ND	0.025 μg g^{-1}	101.0±3.7 %

Note: ND-not detected.

methods, our method of DBDVG realizes vapor reactions through free radicals and electrons in the plasma, with no need to add extra redox reagents such as $HCl/NaBH_4$ in HG or chemical modifiers such as $Pd(NO_3)_2$ in ETV or HCl/HBr in distillation, which greatly lowers the reagent blank. Although the LOD of ^{79}Se by conventional ICP-MS was lower than ICP-MS/MS[22,23] and AMS,[14] the LOD of ^{79}Se achieved by our method using conventional ICP-MS is still sufficient for the analysis of environmental samples contaminated by nuclear waste such as the cut and living tree samples with ^{79}Se activities of 1.5-2.1 Bq g^{-1} (~ 2.6-3.7 ng g^{-1}) collected near Fukushima Daiichi Nuclear Power Station reported in ref 10.

Sample Analysis. As the detection limit of ^{77}Se (LOD of 13 ng L^{-1} and limit of quantification of 44 ng L^{-1}) was similar to ^{79}Se, and minor mass interference was observed for ^{77}Se determination,[15] the concentration of ^{77}Se instead of ^{79}Se in the certified Se isotopic reference material in selenious acid solution (GBW 04457) was diluted and determined by the external standard method to validate the accuracy of the proposed method. The measured concentration of ^{77}Se (15.03 ± 0.13 mg L^{-1}, with the precision of 1.7%) was in good agreement with the certified value (15.2 mg L^{-1}) with the trueness of -1.1%. To further evaluate the application of this proposed method, the concentration of ^{79}Se and ^{77}Se and the recoveries of ^{77}Se in environmental samples such as lake water and plant leaves were also determined. Before analysis by the SPME-DBDVG-AAE-ICP-MS method, lake water sample (50 mL) required filtration and acidification, whereas plant leaves (0.5 g) necessitated digestion with HNO_3-H_2O_2 solution and finally diluted to 50 mL. The detail of the digestion steps was shown in the Supporting Information. Considering the complexity of the sample matrix, standard addition method was used to determine the ^{77}Se concentration in these two samples. And the ^{79}Se concentration was calculated by the eq. (3):

$$[^{79}Se] = [^{77}Se] \cdot (^{79}Se/^{77}Se) \quad (3)$$

where the $[^{79}Se]$ and $[^{77}Se]$ mean the concentration of ^{79}Se and ^{77}Se in the sample, and ($^{79}Se/^{77}Se$) means the net-intensity ratio of ^{79}Se and ^{77}Se determined by SPME- DBDVG-AAE-ICP-MS method. As shown in Table 2, the concentration of ^{77}Se in the lake water and plant leave were 0.055 ± 0.007 μg L^{-1} and 0.0041 ± 0.0003 μg g^{-1}, respectively, while the concentration of ^{79}Se could not be detected in both samples, indicated that these samples were not contaminated by ^{79}Se. Meantime, the recoveries of ^{77}Se in these samples were calculated as 99.9±4.1 % and 101.0±3.7 %, respectively, which also demonstrated the feasibility of this method for ^{77}Se as well as ^{79}Se determination in environmental samples.

CONCLUSION

A new method for ^{79}Se determination in environmental sample was proposed by SPME-DBDVG-AAE-ICP-MS in this work. Unlike HG and ETV sample introduction approaches, our DBDVG system performs the required redox reactions using plasma-generated free radicals and electrons, removing the need for extra redox reagents in HG protocols or chemical modifiers in ETV procedures, and thus markedly cutting down the associated reagent blank. The mass interference of $^{38}Ar^{40}ArH^+$ was effectively eliminated by the addition of He gas in the CRC, and the other potential interferences of $^{39}K^{40}Ar^+$, $^{63}Cu^{16}O^+$, $^{158}Gd^{2+}$, $^{158}Dy^{2+}$ and $^{78}SeH^+$ were all not obvious in this method. Attributed to the enrich and matrix separation process, this method has the

potential to be used for ^{79}Se determination in environmental samples. Nevertheless, the considerable time consumption and procedural complexity associated with this method still need to be addressed and improved in subsequent work.

ASSOCIATED CONTENT

The supporting information (Text S1, Figs. S1-S4, and Table S1) is available at https://www.at-spectrosc.com

AUTHOR INFORMATION

Qian He is an associate professor of environmental analytical chemistry in the key laboratory of marine chemistry theory and technology of ministry of education in Ocean University of China. She received her Ph.D. degree from China University of Geoscience (Wuhan) and successively worked as a postdoctoral researcher at the Tsinghua University (China). Her current research focuses on developing sensitive analytical methods for environmental analysis of trace elements and isotopes.

Corresponding Author

* Q. He

Email address: heqian@ouc.edu.cn

Notes

The authors declare no competing financial interest.

ACKNOWLEDGMENTS

The authors would like to thank gratefully acknowledge the National Nature Science Foundation of China (42306208), the Fundamental Research Funds for the Central Universities of Ocean University of China (202542001 and 202562002) and the Special Projects of Frontiers Science Center for Deep Ocean Multispheres and Earth System of Ocean University of China (202672009).

REFERENCES

1. P. Bienvenu, P. Cassette, G. Andreoletti, M.-M. Bé, J.m. Comte, and M.-C. Lépy, *Appl. Radiat. Isotopes*, 2007, **65**, 355-364. https://doi.org/10.1016/j.apradiso. 2006.09.009
2. G. JöRg, R. Bühnemann, S. Hollas, N. Kivel, K. Kossert, S.V. Winckel, and C.L.V. Gostomski, *Appl. Radiat. Isot.*, 2010, **68**, 2339-2351. https://doi.org /10.1016/ j.apradiso. 2010.05.006
3. M. He, S. Jiang, S. Jiang, L. Diao, S. Wu, and C. Li, *Nucl. Instrum. Methods Phys. Res. B*, 2002, **194**, 393-398. https://doi.org /10.1016/S0168-583X(02)01031-5
4. M. Rose, S. Shaw, K. Morris, C. Boothman, M. Bailey, D. Engelberg and J. R. Lloyd, *Environ. Sci. Technol.*, 2026, **60**, 4124-4133. https://doi.org/10.1021/acs.est.5c09387
5. T. Almahayni, *J. Environ. Radioact.*, 2022, **255**, 107043. https://doi.org/10.1016/ j.jenvrad.2022.107043
6. E. Siasou and N. Willey, *J. Environ. Radioact.*, 2025, **282**, 107622. https://doi.org/ 10.1016/j.jenvrad.2025.107622
7. R.A. Dewberry, J.D. Leyba, and W.T. Boyce, *J. Radioanal. Nucl. Chem.*, 2000, **245**, 491-500. https://doi.org/10.1023/A:1006736621914
8. C. Frechou, S. Aguerre, J.-P. Degros, G. Kerlau, and T. Grangeon, *Talanta* 2007, **72**, 1166-1171. https://doi.org/10.1016/j.talanta.2007.01.011
9. D.P. DiPrete, C.C. DiPrete, N.E. Bibler, C.J. Bannochie, and M.S. Hay, *J. Radioanal. Nucl. Chem.*, 2009, **282**, 663-667. https://doi.org/10.1007/ s10967-009-0274-5
10. K. Tanaka, A. Shimada, A. Hoshi, M. Yasuda, M. Ozawa, and Y. Kameo, *J. Nucl. Sci. Technol.*, 2014, **51**, 1032-1043. https://doi.org/10.1080/00223131. 2014.921583
11. S. Dulanska, B. Horvathova, B. Remenec, and L. Matel, *Appl. Radiat. Isot.*, 2019, **148**, 35-39. https://doi.org/10.1016/j.apradiso.2019.03.027
12. M. He, S. Jiang, S. Jiang, Q. Chen, J. Qin, S. Wu, Y. Dong, and Z. Zhao, *Nucl. Instrum. Methods Phys. Res. B*, 2000, **172**, 177-181. https://doi.org/ 10.1016/S0168-583X(00)00393-1
13. W. Wang, X. Ruan, L. Lu, J. Gong, S. Wu, D. Zhang, M. He, and S. Jiang, *Nucl. Instrum. Methods Phys. Res. B*, 2010, **268**, 764-768. https://doi.org/ 10.1016/j.nimb.2009.10.025
14. W. Wang, Y. Guan, M. He, S. Jiang, S. Wu, and C. Li, *Nucl. Instrum. Methods Phys. Res. B*, 2010, **268**, 759-763. https://doi.org/10.1016/j.nimb.2009.10.024
15. J. Comte, P. Bienvenu, E. Brochard, J.M. Fernandez, and G. Andreoletti, *J. Anal. At. Spectrom.*, 2003, **18**, 702-707. https://doi.org/10.1039/b209253k
16. S. Aguerre and C. Frechou, *Talanta* 2006, **69**, 565-571. https://doi.org/ 10.1016/j.talanta.2005.10.028
17. K. Hoppstock, J.S. Becker, and H.J. Dietze, *At. Spectrosc*., 1997, **18**, 180-185.
18. S. Asai, Y. Hanzawa, K. Okumura, N. Shinohara, J. Inagawa, S. Hotoku, K. Suzuki, and S. Kaneko, *J. Nucl. Sci. Technol.*, 2011, **48**, 851-854. https://doi.org/10.3327/jnst.48.851
19. S. Asai, Y. Hanzawa, K. Okumura, N. Shinohara, J. Inagawa, S. Hotoku, K. Suzuki and S. Kaneko, *J. Nucl. Sci. Technol.*, 2011, **48**, 851-854. https://doi.org/10.1080/18811248.2011. 9711768
20. C. D. Pereira, M. Á. Aguirre, J. A. Nóbrega, M. Hidalgo and A. Canals, *Microchem. J.*, 2014, **112**, 82-86. http://dx.doi.org/10.1016/j.microc.2013.09.006
21. M. García1, M. Á. Aguirre1, A. Canals, *Anal. Bioanal. Chem*., 2017, **409**, 5481-5490. https://doi.org/10.1007/s00216-017-0484-6
22. I.M. Banjarnahor, V.-K. Do, T. Furuse, Y. Ohta, and K. Tanaka, *J. Radioanal. Nucl. Chem.*, 2025, **334**, 4997-5006. https://doi.org/10.1007/s10967-025-10143-w
23. S.T. Lancaster, B. Russell, T. Prohaska, and J. Irrgeher, *J. Anal. At. Spectrom.*, 2025, **40**, 3210-3220. https://doi.org/10.1039/d5ja00254k
24. R. Brennetot, L. Pierry, T. Atamyan, G. Favre and D. Vailhen, *J. Anal.*

At. Spectrom., 2008, **23**, 1350-1358. https://doi.org/10.1039/b802820f

25. M. Guidotti and G. Ravaioli, *J. High Resol. Chromatogr*., 1999, **22**, 414-416. https://doi.org/10.1002/(SICI)1521-4168(19990701)22:7<414::AID-JHRC414>3.0.CO;2-J
26. X. Liu, Z. Zhu, Z. Bao, D. He, H. Zheng, Z. Liu, and S. Hu, *Anal. Chem.* 2019, **91**, 928-934. https://doi.org/10.1021/acs.analchem.8b03966
27. S. Chen, R. Wang, Z. Zhu, X. Kong, and Q. He, *Spectrochim. Acta Part B*, 2025, **234**, 107343. https://doi.org/10.1016/j.sab.2025.107343
28. L. Wang and X. Xu, *New J. Chem*., 2022, **46**, 12720-12728. https://doi.org/ 10.1039/d2nj02211g
29. X. Wu, X. Guo, and L. Zhang, *Ind. Eng. Chem. Res.*, 2019, **58**, 342-349. https://doi.org/10.1021/acs.iecr.8b04288
30. R. Wang, S. Chen, Q. He, and S. Xu, *Anal. Chem*. 2024, **96**, 17405-17412. https://doi.org/10.1021/acs.analchem.4c04340
31. X. Liu, Z.L. Zhu, P.J. Xing, H.T. Zheng, and S.H. Hu, *Spectrochim. Acta Part B*, 2020, **167**, 105822. https://doi.org/10.1016/j.sab.2020.105822
32. X. Wu, X. Guo, and L. Zhang, *Ind. Eng. Chem. Res*., 2019, **58**, 342-349. http://dx.doi.org/10.1021/acs.iecr.8b04288
33. M. Yang, J. Xue, M. Li, G. Han, Z. Xing, S. Zhang, and X. Zhang, *Talanta*, 2014, **126**, 1-7. http://dx.doi.org/10.1016/j.talanta.2014.03.009
34. M. Li, Z. Xing, G. Sun, J. Liang, X. Huang, B. Fan, and Q. Wang. *J. Anal. At. Spectrom*. 2020, **35**, 904-911. https://doi.org/10.1039/d0ja00005a
35. https://www.nemi.gov/methods/method_pdf/4777/?utm_source=chatgpt.com